NASA TR R-150

NATIONAL AERONAUTICS AND SPACE ADMINISTRATION

TECHNICAL REPORT
R-150

THEORETICAL STUDY OF CAMBER FLUTTER CHARACTERISTICS OF MONOCOQUE AND MULTIWEB WINGS

By ROBERT G. THOMSON and EDWIN T. KRUSZEWSKI

1962

TECHNICAL REPORT R-150

THEORETICAL STUDY OF CAMBER FLUTTER CHARACTERISTICS OF MONOCOQUE AND MULTIWEB WINGS

By ROBERT G. THOMSON and EDWIN T. KRUSZEWSKI

Langley Research Center
Langley Station, Hampton, Va.

TECHNICAL REPORT R-150

THEORETICAL STUDY OF CAMBER FLUTTER CHARACTERISTICS OF MONOCOQUE AND MULTIWEB WINGS

By Robert G. Thomson and Edwin T. Kruszewski

SUMMARY

A theoretical flutter analysis has been made that utilizes the same simplified model employed in the vibrational investigation presented in TN D-987 in which chordwise and spanwise flexibilities of the actual wing are duplicated. This idealized model subjected to a supersonic flow is investigated to predict the flutter behavior and establish a flutter boundary. Additional effects such as aerodynamic damping and variations in cross-sectional curvature are determined and their effect on the predicted flutter boundary ascertained. A comparison of the predicted flutter boundary with results obtained experimentally for multiweb wing structures shows very good agreement.

INTRODUCTION

In an experimental investigation conducted by the Langley Structures Research Division into the dynamic flutter failures of multiweb wing structures, chordwise or camber flutter was found to be a primary mode of failure when insufficient bulkheads were used. This flutter consisted of small-amplitude oscillations with five or less spanwise node lines across the chord. In the investigation a series of multiweb wing structures were tested in the preflight jet of the NASA Wallops Station at a Mach number of 2 as discussed in references 1, 2, and 3. Additional tests have also been made in the Langley 9- by 6-foot thermal structures tunnel at a Mach number of 3, and these flutter data are included also. These multiweb models had 5-percent-thick circular-arc airfoil sections containing six webs and a solid leading and trailing edge. In attempts to predict this flutter behavior theoretically, modal approaches using the lowest five experimental mode shapes have not been very successful. Vibration behavior of such structures, however, has been successfully predicted theoretically (for example, ref. 4) by the use of an analysis of a simplified model which took cognizance of the cross-sectional flexibilities. Hence, the same idealized model subjected to a supersonic flow has been investigated in an attempt to obtain a method of predicting the flutter behavior of the multiweb wings. D. J. Johns, in a note on the influence of panel deformations on wing flutter (ref. 5), also recognized the significance of coupling between cross-sectional and spanwise deformation modes. This analysis, however, was applicable only to wings with rectangular cross sections and consequently did not include any effects of curvature of the cross section.

The purpose of the present paper is to present the results of a flutter analysis of the idealized structure and to show how these results can be used to predict the flutter behavior of multiweb and monocoque low-aspect-ratio wings of circular-arc cross section. The idealized structure consists of a typical cross section of the wing mounted on springs and hence embodies the principal mechanisms of the cross-sectional and spanwise flexibilities of the actual wing. A modified linear piston theory is used to represent the aerodynamic forces created by supersonic flow. The analysis consists in solving the basic equations by means of a Galerkin procedure using a modal approximation of three and four terms but neglecting the effect of aerodynamic damping. The accuracy of this Galerkin procedure is determined in two ways — first, by the apparent convergence of the results of the three- and four-term solutions and second, by a comparison of the flutter boundaries for the case of the idealized structure with infinitely stiff spring supports (pin-ended) at the leading and trailing edges as calculated by the Galerkin method

with those obtained from an exact analysis. In addition, the effects of damping are evaluated by a two-mode Galerkin solution that includes the effects of aerodynamic damping. Finally, the results of the analysis are used to predict successfully the flutter boundary of the multiweb wings used in the experimental investigations.

SYMBOLS

$B=\left(3\,\frac{qc^4}{E\beta t^3 U_\infty}\,i\omega-\alpha^4\right)^{1/4}$

c chord length of beam

E modulus of elasticity

h distance from x-axis to median line of skin

h_0 value of h at $x=0$

I area moment of inertia about median line of skin, per unit length, $t^3/12$

I_p area polar moment of inertia per unit length, $I_{xx}+I_{yy}$

j, l integers

k spring constant

M Mach number

m roots of auxiliary equation (see appendix)

q dynamic pressure, $\frac{1}{2}\rho_\infty U_\infty^2$

t skin thickness

U_∞ free-stream velocity

w amplitude of deflection in z-direction (positive upward)

$\bar{w}$ deflection in z-direction, $\mathrm{Re}(we^{i\omega\tau})$

x, y, z Cartesian coordinates (fig. 1)

α frequency coefficient, $\left(\frac{c^4\rho t\omega^2}{16EI}\right)^{1/4}$

$\beta=\sqrt{M^2-1}$

$\gamma, \delta, \theta, \phi$ assumed coefficients of the roots of the exact equation (see eqs. (A9) of appendix)

Λ dynamic-pressure parameter, $\frac{3q}{E\beta}\left(\frac{c}{t}\right)^3$

Λ_{cr} critical value of Λ

λ amplitude of normal midplane force in the beam (positive in tension)

$\bar{\lambda}$ normal midplane force, $\mathrm{Re}(\lambda e^{i\omega\tau})$

μ Poisson's ratio

$\xi=\frac{2x}{c}$

ρ mass density of cover

ρ_∞ mass density of air (free stream)

τ time

$\psi=\xi+1$

ω natural frequency

Subscripts:

A antisymmetrical

i, m, n any integer

S symmetrical

T torsional

x, y, z, τ variable with respect to which primary symbol is differentiated

Primes and superscript IV on symbols denote differentiation with respect to ξ.

ANALYSIS

IDEALIZED STRUCTURE

A rigorous approach to the flutter analysis of the multiweb wing shown in figure 1(a) would, of necessity, involve some type of shell analysis and sophisticated aerodynamics. A more convenient though less rigorous approach is to investigate an idealized structure identical to that used in the vibration analysis of reference 4. The only structures considered are those that have relatively uniform properties in the spanwise direction with a doubly symmetrical curved airfoil cross section as shown in figure 1(a). The wing or beam is assumed to be of either pure monocoque or multiweb cross section with no or relatively few internal ribs.

The idealized structure consists of a typical cross section of the wing mounted on identical elastic supports as shown in figure 1(b). The cross section consists of two curved uniform beams attached at the ends in such a manner as to maintain the angle between the beams at each end. The rigid-body motion of the idealized structure depends on the stiffness of the elastic supports which simulate the beam bending and torsional stiffness of the wing. The depth of the individual beams in the idealized structure is taken to be the same as the thickness t of the covers in the prototype. The curvature of the covers of the wings considered is such as can be represented by the parabolic equation $h=h_0(1-\xi^2)$ where h_0 is the maximum value of h and ξ is the nondimensional coordinate $2x/c$.

The webs of the multiweb structure are assumed to contribute nothing to the camber stiffness. They do, however, tend to prevent any relative motion between the top and bottom covers. Thus, the additional assumption is made that the deflections of the top and bottom beams in the idealized structure are the same. Each beam of the idealized structure is permitted to carry midplane forces

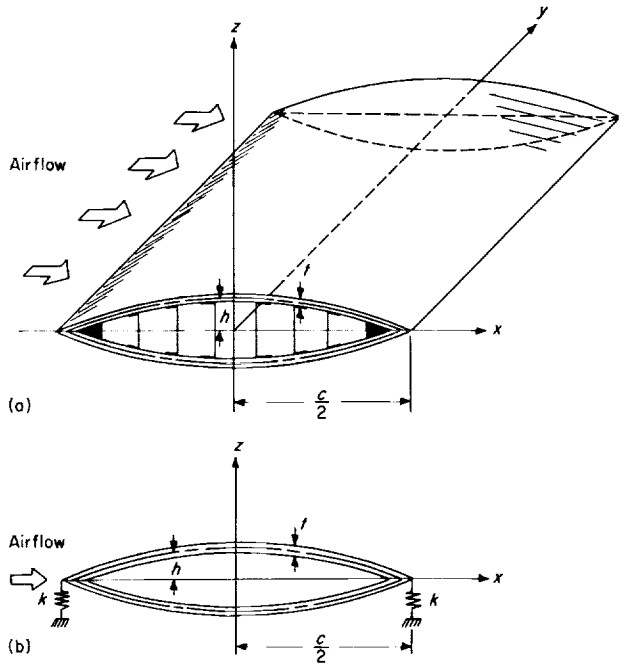

(a) Prototype.

(b) Idealization.

FIGURE 1.- Low-aspect-ratio multiweb wing.

in addition to transverse shear forces and bending moments and is considered to be acting in a manner consistent with elementary theory (i.e., plane sections remain plane). The air loads to which the idealized structure are subjected are taken as those given by modified linear piston theory.

GOVERNING EQUATIONS

The appropriate differential equation and boundary conditions for the idealized structure shown in figure 1(b) for the deflection $\overline{w}$ are

$$EI\overline{w}_{xxxx}-\overline{\lambda}h_{xx}+\rho t\overline{w}_{\tau\tau}=-\frac{2q}{\beta}\overline{w}_x-\frac{2q}{\beta U_\infty}\overline{w}_\tau \tag{1}$$

$$\overline{w}_{xx}\Big|_{x=\frac{c}{2}}=\overline{w}_{xx}\Big|_{x=-\frac{c}{2}}=0 \tag{2}$$

$$EI\overline{w}_{xxx}-\overline{\lambda}h_x-\frac{k}{2}w\Big|_{x=\frac{c}{2}}=0 \tag{3}$$

$$EI\overline{w}_{xxx}-\overline{\lambda}h_x+\frac{k}{2}w\Big|_{x=-\frac{c}{2}}=0 \tag{4}$$

where

U_∞ free-stream velocity

q dynamic pressure, $\frac{1}{2}\rho_\infty U_\infty^2$

β compressibility factor, $\sqrt{M^2-1}$

and the subscripts x and τ denote differentiation with respect to x and τ. The midplane force $\overline{\lambda}$, as in reference 4, was assumed constant over the length of the beam (for any finite τ) and an integral expression for $\overline{\lambda}$ was arrived at by the assumption that no overall shortening or lengthening of the beams was possible. Thus,

$$\overline{\lambda}=\frac{Et}{c}\int_{-c/2}^{c/2}h_x\overline{w}_x dx \tag{5}$$

Note that when $\overline{w}$ is antisymmetrical, the integrand of equation (5) is an antisymmetrical function about the midchord ($x=0$); consequently, its integral from $-c/2$ to $c/2$ is zero and no midplane forces are present. This is not true for the symmetrical case.

The differential equation and associated boundary conditions are similar to equations (9) to (13) of reference 4 except that terms are included on the right-hand side of equation (1) to represent the air loads given by modified linear piston theory (modified in the sense that $1/M$ is replaced by $1/\beta$). The first term on the right-hand side of the modified-piston-theory equation (1) is a static-loading term and the second an aerodynamic damping term. The solution of equation (1) can be written in the form

$$\overline{w}=\mathrm{Re}\,[w(x)e^{i\omega\tau}] \tag{6}$$

$$\overline{\lambda}=\mathrm{Re}\,[\lambda e^{i\omega\tau}] \tag{7}$$

From equations (6) and (7) it can be seen that stable motion is assured as long as the imaginary part of the frequency ω is zero or positive. Hence, the flutter boundary is defined as the lowest value of q at which the imaginary part of any ω becomes negative and therefore in the ensuing analysis only real values of ω are considered.

Substituting equations (6) and (7) into equation (1) and the associated boundary conditions, using the parabolic equation $h=h_0(1-\xi^2)$ together with $I=\frac{t^3}{12}$, and nondimensionalizing yields

$$w^{IV}+\Lambda w'+B^4 w=-\frac{6\lambda h_0 c^2}{Et^3} \tag{8}$$

$$w''|_{\xi=1}=w''|_{\xi=-1}=0 \tag{9}$$

$$w'''+\frac{6h_0\lambda c^2}{Et^3}\xi-\frac{3}{4}\frac{k}{E}\left(\frac{c}{t}\right)^3 w\Big|_{\xi=1}=0 \tag{10}$$

$$w'''+\frac{6h_0\lambda c^2}{Et^3}\xi+\frac{3}{4}\frac{k}{E}\left(\frac{c}{t}\right)^3 w\Big|_{\xi=-1}=0 \tag{11}$$

where the primes and the superscript IV denote differentiation with respect to $\xi=\frac{2x}{c}$, and Λ is a dynamic-pressure parameter defined as

$$\Lambda=\frac{3q}{E\beta}\left(\frac{c}{t}\right)^3 \tag{12}$$

A frequency parameter B^4 is defined as

$$B^4=\frac{3}{2}\frac{qc^4}{E\beta t^3 U_\infty}i\omega-\alpha^4 \tag{13}$$

$$\alpha^4=\frac{3c^4\rho\omega^2}{4Et^2} \tag{14}$$

and

$$\lambda=\frac{2Et}{c^2}\int_{-1}^{1}h'w'd\xi=\frac{4Eth_0}{c^2}\left(-\xi w\Big|_{-1}^{1}+\int_{-1}^{1}w d\xi\right) \tag{15}$$

EXACT SOLUTION

An exact solution to equation (1) in which aerodynamic damping has been neglected is obtained in this section. The approach is similar to that used in reference 6, which presents an exact solution for panel flutter of a simply supported plate. Although solutions of the flutter of the idealized structure considered in this section are possible for any value of spring constant k, only the special case of infinite k is presented. This approach results in considerable simplification in boundary conditions and consequent numerical procedures; for example, the solutions are not dependent on values of c/t or E. Although considerably simplified, the solution still provides a means of evaluating the effect of curvature and its associated normal midplane force λ on flutter behavior. These are the principal effects that distinguish the present analysis from typical wing-flutter or panel-flutter studies. If no initial curvature is present as in the case of a straight beam, h_0 is considered zero and consequently λ is zero, and the differential equation and boundary conditions are identical to that given in reference 7 for an infinite-aspect-ratio plate (with the exception of a factor of $\frac{1}{1-\mu^2}$ resulting from the use of the plate stiffness D in the panel analysis and EI in the beam analysis).

If the aerodynamic damping is neglected, the last term in equation (1) is omitted and the expression for B^4 given by equation (13) reduces to $-\alpha^4$. The solution to this differential equation and boundary conditions is discussed in the appendix. In the appendix it is shown that the deflection w can be written as

$$w=\frac{6\lambda h_0 c^2}{\alpha^4 Et^3}+e^{\theta\psi}(C_1\cosh\phi\psi+C_2\sinh\phi\psi)+e^{-\theta\psi}(C_3\cos\delta\psi+C_4\sin\delta\psi) \tag{16}$$

where the relations between ϕ, δ, α^4, and θ are given by the following equations:

$$\phi^2=-\theta^2-\frac{\Lambda}{4\theta} \tag{17}$$

$$\delta^2=\theta^2-\frac{\Lambda}{4\theta} \tag{18}$$

$$\alpha^4=\frac{\Lambda^2}{16\theta^2}-4\theta^4 \tag{19}$$

In addition

$$\left.\begin{array}{l}-\frac{\Lambda^{1/3}}{2}<\theta<0\\ |\phi|>|\theta|\end{array}\right\} \tag{20}$$

Substitution of equation (16) into the boundary conditions (eqs. (A4) and (A5)) results in the characteristic equation presented in table I. Although as written in table I the determinant is a function of θ, ϕ, δ, α, Λ, and $\left(\frac{t}{h_0}\right)^2$, the parameters ϕ, δ, and α can in turn be written as functions of θ and Λ. (See eqs. (17) to (19).) Consequently the determinant can be considered as a function of only θ, Λ, and $\left(\frac{t}{h_0}\right)^2$. For a given value of Λ and $\left(\frac{t}{h_0}\right)^2$ the appropriate value of θ can be determined from the characteristic equation. The corresponding value of α can then be computed from equation (19).

TABLE I.—FLUTTER DETERMINANT OF EXACT SOLUTION, WHEN $k=\infty$ AND AERODYNAMIC DAMPING IS NEGLECTED

$$\begin{vmatrix} 1+aH_1 & aH_2 & 1+aH_3 & aH_4 \\ (\theta^2+\phi^2) & 2\theta\phi & (\theta^2-\delta^2) & -2\theta\delta \\ e^{2\theta}\cos 2\phi-1 & e^{2\theta}\sin 2\phi & e^{-2\theta}\cos 2\delta-1 & e^{-2\theta}\sin 2\delta \\ H_5 & H_6 & H_7 & H_8 \end{vmatrix}=0$$

where

$$a=\frac{1}{2\vartheta\left[\frac{\alpha^4}{48}\left(\frac{t}{h_0}\right)^2-1\right]}$$

$$H_1=\frac{e^{2\theta}\left(\cos 2\phi-\frac{\phi}{\theta}\sin 2\phi\right)-1}{1-\left(\frac{\phi}{\theta}\right)^2}$$

$$H_2=\frac{e^{2\theta}\left(\sin 2\phi-\frac{\phi}{\theta}\cos 2\phi\right)+\frac{\phi}{\theta}}{1-\left(\frac{\phi}{\theta}\right)^2}$$

$$H_3=\frac{e^{-2\theta}\left(-\cos 2\delta+\frac{\delta}{\theta}\sin 2\delta\right)+1}{1+\left(\frac{\delta}{\theta}\right)^2}$$

$$H_4=\frac{e^{-2\theta}\left(-\sin 2\delta-\frac{\delta}{\theta}\cos 2\delta\right)+\frac{\delta}{\theta}}{1+\left(\frac{\delta}{\theta}\right)^2}$$

$$H_5=e^{2\theta}[(\theta^2+\phi^2)\cos 2\phi+2\theta\phi\sin 2\phi]$$

$$H_6=e^{2\theta}[(\theta^2+\phi^2)\sin 2\phi+2\theta\phi\cos 2\phi]$$

$$H_7=e^{-2\theta}[(\theta^2-\delta^2)\cos 2\delta+2\theta\delta\sin 2\delta]$$

$$H_8=e^{-2\theta}[(\theta^2-\delta^2)\sin 2\delta-2\theta\delta\cos 2\delta]$$

$$\alpha^4=\frac{\Lambda^2}{16\theta^2}-4\theta^4$$

In figure 2 a plot of the dynamic-pressure parameter Λ as a function of the frequency parameter α is shown by the solid curves for $\left(\frac{t}{h_0}\right)^2=0$. For discrete values of Λ an infinite set of values of α is shown to exist. When Λ equals zero, the values of α correspond to the natural vibration frequencies determined in reference 4 for a monocoque beam in a vacuum. As Λ increases from zero, these natural frequencies change until a value of Λ is reached in which two of the roots of α coalesce. For values of Λ greater than this value two of the values of α become complex and hence, as can be seen from equation (14), ω will be complex. Since ω must remain real to give stable oscillatory motion, this value of Λ is the critical value Λ_{cr} and thus defines the flutter boundary. In figure 3, Λ_{cr} is plotted as a function of $\left(\frac{t}{h_0}\right)^2$ from 0 to 0.25. Note that $\left(\frac{t}{h_0}\right)^2$ for all practical configurations is much less than unity. For example, in an extreme case where the skin thickness is equal to half the value of h_0, this ratio is only 0.25. In the more practical type of construction of multiweb wings such as those presented in references 1, 2, and 3 the ratio $\left(\frac{t}{h_0}\right)^2$ is in the range of 0.020. Consequently, within the range of practical design of multiweb and monocoque wings the ratio $\left(\frac{t}{h_0}\right)^2$

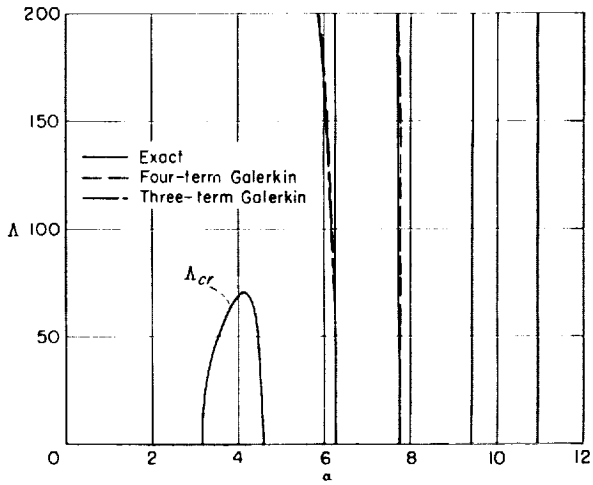

FIGURE 2.—Effect of dynamic-pressure parameter on pinended ($k=\infty$) wing frequencies for $\left(\frac{t}{h_0}\right)^2=0$.

$\alpha=\left(\frac{3c^4\rho\omega^2}{4Et^2}\right)^{1/4}$; $\Lambda=\frac{3q}{E\beta}\left(\frac{c}{t}\right)^3$.

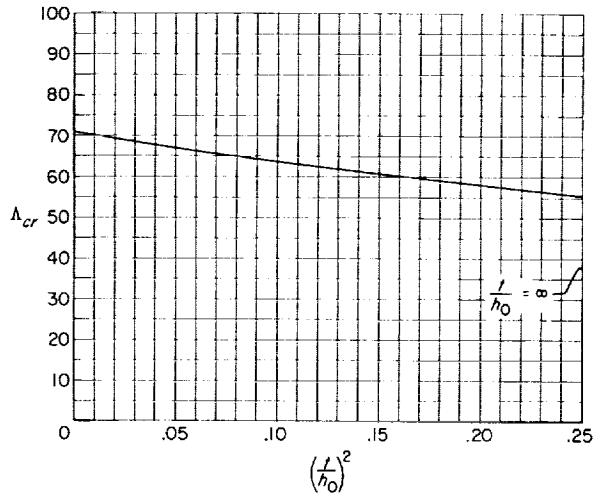

Figure 3. Effect of variation in $\left(\frac{t}{h_0}\right)^2$ on Λ_{cr} for exact solution. $k=\infty$.

can be assumed to approach zero without appreciably affecting the value of Λ_{cr}. For this reason in the analysis performed by the Galerkin procedure in the next section, a constant value of $\left(\frac{t}{h_0}\right)^2=0$ is used as this assumption results in considerable simplification in the numerical computations. Although, as was previously discussed, $\left(\frac{t}{h_0}\right)^2$ for all practical cases is much less than one, a unique situation occurs in the limiting case where the two curved beams merge into a straight beam. For this limiting case h_0 is assumed to be zero and $\left(\frac{t}{h_0}\right)^2\to\infty$. It can be shown that for this case the differential equation and boundary conditions (eqs. (1), (A4), and (A5)) limit to the equations presented in reference 7 for the infinite-aspect-ratio flat panel. The value of Λ_{cr} for $\left(\frac{t}{h_0}\right)^2=\infty$ is 37.96 and is indicated in figure 3 in order to compare the effects of cross-sectional curvature and its associated midplane forces with flat-panel results containing no in-plane forces. Comparing this value of Λ_{cr} with that calculated for $\left(\frac{t}{h_0}\right)^2=0$ ($\Lambda_{cr}=70.9$) demonstrates that the existence of curvature can have appreciable effect on the flutter criterion. However, as can be seen from figure 3, once the curvature is present, variations in the degree of curvature can have little effect on the final flutter boundary.

SOLUTIONS BY THE GALERKIN PROCEDURE

The previous solution, although exact, was for the special case of pin-ended constraint conditions where $k=\infty$. In order to study the effect of spanwise flexibility on the overall motion of the idealized structure finite values of the elastic supports must be used. Because of the resulting complexity in the final determinant which occurs in the case of an exact solution, a Galerkin procedure using a theoretical modal approach is used to determine the flutter characteristics. As was done in the exact solution, the effects of aerodynamic damping are neglected. The importance of this effect is discussed in a subsequent section.

In order to perform a Galerkin solution by a modal approach, the choice of modes to be applied must satisfy both the geometric boundary conditions and the natural boundary conditions. Since the inclusion of the dynamic pressure q in equation (1) does not alter the boundary conditions associated with the elastic supports, the mode shapes and frequencies of the vibrational analysis of such structures derived in reference 4 are used in the Galerkin procedure. That is, the deflection is represented by

$$w=a_0w_{0,S}+\sum_{n=1}^{j}a_nw_{n,S}+\sum_{m=0}^{l}b_mw_{m,A} \qquad (21)$$

where $w_{0,S}$, $w_{n,S}$, and $w_{m,A}$ are the symmetric and antisymmetric vibration modes. Note that the coefficients a_0, a_n, and b_m can be complex but $w_{0,S}$, $w_{n,S}$, and $w_{m,A}$ are real. The mode shapes $w_{n,S}$ and $w_{m,A}$ and their associated frequency equations have been derived in reference 4 for all values of t/h_0. Examination of the equations given in reference 4 shows that a significant simplification results when t/h_0 approaches zero. Inasmuch as the exact solution has shown that this simplifying assumption would have no appreciable effect on the resulting flutter boundary for $k=\infty$, t/h_0 is assumed to be zero, whereas c/t remains finite. The frequency equation for the symmetrical case as obtained from reference 4 for $\left(\frac{t}{h_0}\right)^2=0$ becomes

$$2\alpha_{n,S}=\tan\alpha_{n,S}+\tanh\alpha_{n,S} \qquad (22)$$

and the associated mode shape is written as

$$w_{n,S}=\frac{\cos\alpha_{n,S}\xi}{\cos\alpha_{n,S}}+\frac{\cosh\alpha_{n,S}\xi}{\cosh\alpha_{n,S}}-2 \qquad (23)$$

where

$$\alpha_{n,S}=\left(\frac{3c^4\rho\omega_{n,S}^2}{4Et^2}\right)^{1/4} \tag{24}$$

For the antisymmetrical modes, as was previously discussed, the midplane force λ is zero, and the differential equation of vibration simply reduces to the elementary beam equation. Thus, the characteristic or frequency equation can be written as

$$\frac{\coth \alpha_{m,A}-\cot \alpha_{m,A}}{2\alpha_{m,A}}=\frac{3k}{4E\alpha_{m,A}^4}\left(\frac{c}{t}\right)^3 \tag{25}$$

and the mode shape is

$$w_{m,A}=\frac{\sin \alpha_{m,A}\xi}{\sin \alpha_{m,A}}+\frac{\sinh \alpha_{m,A}\xi}{\sinh \alpha_{m,A}} \tag{26}$$

where

$$\alpha_{m,A}=\left(\frac{3c^4\rho\omega_{m,A}^2}{4Et^2}\right)^{1/4} \tag{27}$$

It can be shown by the use of the general mode shapes given in reference 4 that regardless of the value of $\left(\frac{t}{h_0}\right)^2$, the natural vibration modes are orthogonal for all values of k. Consequently,

$$\int_{-1}^{1} w_{n,S}w_{i,S}d\xi=0 \qquad (i\neq n)\begin{cases}(n=0,1,2,\ldots j)\\(i=0,1,2,\ldots j)\end{cases} \tag{28}$$

$$\int_{-1}^{1} w_{n,S}w_{m,A}d\xi=0 \qquad \begin{cases}(n=0,1,2,\ldots j)\\(m=0,1,2,\ldots l)\end{cases} \tag{29}$$

$$\int_{-1}^{1} w_{m,A}w_{i,A}d\xi=0 \qquad (i\neq m)\begin{cases}(i=0,1,2,\ldots l)\\(m=0,1,2,\ldots l)\end{cases} \tag{30}$$

Note from equation (23) that for $\left(\frac{t}{h_0}\right)^2=0$, the tip deflections of the cross section in the symmetrical modes are zero and

$$\int_{-1}^{1} w_{n,S}d\xi=0 \qquad (n=1,2,\ldots j) \tag{31}$$

and

$$\int_{-1}^{1} w'_{m,A}w_{n,S}d\xi=-\int_{-1}^{1} w_{m,A}w'_{n,S}d\xi \qquad \begin{cases}(n=1,2,\ldots j)\\(m=0,1,2,\ldots l)\end{cases} \tag{32}$$

In addition, with the use of equations (23) and (26) the following relationships are obtained

$$\int_{-1}^{1} w_{n,S}^2d\xi=\tan^2 \alpha_{n,S}-\tanh^2 \alpha_{n,S} \qquad (n=0,1,2,\ldots j) \tag{33}$$

$$\int_{-1}^{1} w_{m,A}^2d\xi=2+\cot^2 \alpha_{m,A}-\coth^2 \alpha_{m,A}+\frac{4.5k}{E\alpha_{m,A}^4}\left(\frac{c}{t}\right)^3 \qquad (m=0,1,2,\ldots l) \tag{34}$$

$$\int_{-1}^{1} w_{m,A}w'_{n,S}d\xi=\frac{8\alpha_{n,S}^4}{\alpha_{m,A}^4-\alpha_{n,S}^4}(\alpha_{m,A}\coth \alpha_{m,A}-1)+\frac{6k}{E}\left(\frac{c}{t}\right)^3\left(\frac{\alpha_{n,S}^2}{\alpha_{m,A}^4+\alpha_{m,A}^2\alpha_{n,S}^2}-\frac{\alpha_{n,S}\tan \alpha_{n,S}}{\alpha_{m,A}^4-\alpha_{n,S}^4}\right) \qquad \begin{cases}(m=0,1,2,\ldots l)\\(n=0,1,2,\ldots j)\end{cases} \tag{35}$$

The first mode, $w_{0,S}$, associated with a_0 in equation (21) is the rigid-body translational mode while $w_{0,A}$ consists of predominantly rigid-body torsional or pitching motion; that is, motion of the cross section as a rigid body mounted on spring supports. The rigid-body torsional mode is always the lowest of the antisymmetrical modes, while the rigid-body translational mode is not necessarily the lowest of the symmetric modes. (See ref. 4.) The rest of the modes associated with a_n and b_m are predominantly cross sectional in nature containing two or more nodal points.

By application of the Galerkin procedures and use of the simplifying orthogonality relations given by equations (28) to (30) and equations (31) and (32) for $\left(\frac{t}{h_0}\right)^2=0$, a set of equations for the coefficients a_n and b_m are found. The set of

equations for the coefficients a_n and b_m are:

$$\left.\begin{aligned}
&(\alpha_{0,S}^4-\alpha^4)a_0\int_{-1}^{1}w_{0,S}^2\,d\xi=0 \\
&(\alpha_{n,S}^4-\alpha^4)a_n\int_{-1}^{1}w_{n,S}^2\,d\xi-\Lambda\sum_{m=0}^{l}b_m\int_{-1}^{1}w_{m,A}w'_{n,S}\,d\xi=0 \qquad \begin{cases}(n=1,2,\ldots j)\\(m=0,1,2,\ldots l)\end{cases} \\
&(\alpha_{m,A}^4-\alpha^4)b_m\int_{-1}^{1}w_{m,A}^2\,d\xi+\Lambda\sum_{n=1}^{j}a_n\int_{-1}^{1}w_{m,A}w'_{n,S}\,d\xi=0 \qquad \begin{cases}(m=0,1,2,\ldots l)\\(n=1,2,\ldots j)\end{cases}
\end{aligned}\right\} \tag{36}$$

It can be seen from equations (36) that (at least in the absence of aerodynamic damping) the rigid-body symmetrical (translational) mode $w_{0,S}$ becomes uncoupled in the solution. Furthermore, it can be shown from equations (36) that if the expansion for w in equation (21) contains either all symmetric or all antisymmetric modes, the resulting solutions do not yield an instability; hence, flutter occurs only through the coupling of symmetric and antisymmetric modes. For a nontrivial solution, the determinant of the coefficients must be equal to zero.

Three-term solution.—For a three-term approximation in which the rigid-body torsional mode and the first two cross-sectional modes are considered, the determinant of equations (36) reduces to

$$\begin{vmatrix}
(\alpha_{1,S}^4-\alpha^4)\displaystyle\int_{-1}^{1}w_{1,S}^2\,d\xi & -\Lambda\displaystyle\int_{-1}^{1}w_{1,A}w'_{1,S}\,d\xi & -\Lambda\displaystyle\int_{-1}^{1}w_{2,A}w'_{1,S}\,d\xi \\
\Lambda\displaystyle\int_{-1}^{1}w_{1,A}w'_{1,S}\,d\xi & (\alpha_{1,A}^4-\alpha^4)\displaystyle\int_{-1}^{1}w_{1,A}^2\,d\xi & 0 \\
\Lambda\displaystyle\int_{-1}^{1}w_{2,A}w'_{1,S}\,d\xi & 0 & (\alpha_{2,A}^4-\alpha^4)\displaystyle\int_{-1}^{1}w_{2,A}^2\,d\xi
\end{vmatrix}=0 \tag{37}$$

which upon expansion gives

$$\Lambda^2=\frac{(\alpha_{1,S}^4-\alpha^4)(\alpha_{1,A}^4-\alpha^4)(\alpha_{2,A}^4-\alpha^4)\displaystyle\int_{-1}^{1}w_{1,S}^2\,d\xi\int_{-1}^{1}w_{1,A}^2\,d\xi\int_{-1}^{1}w_{2,A}^2\,d\xi}{(\alpha^4-\alpha_{1,A}^4)\left(\displaystyle\int_{-1}^{1}w_{2,A}w'_{1,S}\,d\xi\right)^2\int_{-1}^{1}w_{1,A}^2\,d\xi+(\alpha^4-\alpha_{2,A}^4)\left(\displaystyle\int_{-1}^{1}w_{1,A}w'_{1,S}\,d\xi\right)^2\int_{-1}^{1}w_{2,A}^2\,d\xi} \tag{38}$$

The variation of the frequency parameter α for finite values of the dynamic-pressure parameter Λ can be obtained from equation (38) by choosing values of α and solving for Λ. Equation (38) also is a function of the wing material E, chord-thickness ratio c/t, and the spring constant k as can be seen from the values given for the integrals (eqs. (33) to (35)). In figure 2 a plot of Λ as a function of α is shown for the three-term Galerkin approximation (by the long-short dashed curves) for $\left(\frac{t}{h_0}\right)^2=0$ and $k=\infty$. As in the case of the exact solution the critical value of Λ is the lowest value of Λ at which two of the frequency parameters α coalesce.

The critical value of Λ, expressed in the form of the often used panel flutter parameter $\frac{t}{c}\left(\frac{E\beta}{q}\right)^{1/3}=\left(\frac{3}{\Lambda_{cr}}\right)^{1/3}$ is shown plotted in figure 4 as a function of k, for an aluminum-alloy ($E=10.6\times10^6$ psi) wing of chord length c of 20 inches and a ratio c/t of 312.5. This ratio c/t was chosen as it corresponds to the ratio for the multiweb wings used in the experimental investigations. The effect of varying c/t on the final flutter boundary will be discussed in a forthcoming section. The region above the computed curve represents the region of stability while the region below represents the region where flutter will occur.

In order to convert the abscissa in figure 4 to a nondimensional form, the results of figure 4 were

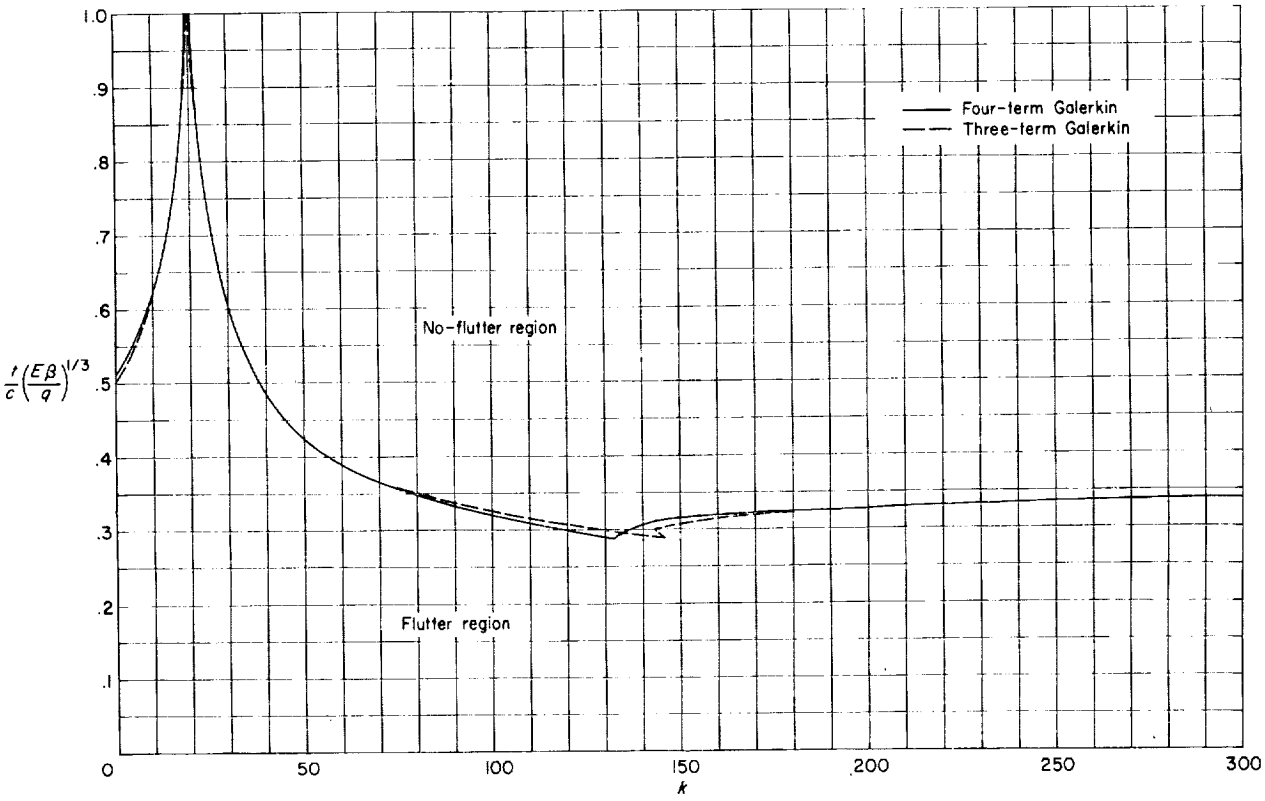

Figure 4.— Variation of the flutter parameter, $\frac{t}{c}\left(\frac{E\beta}{q}\right)^{1/3}$ with k for an aluminum-alloy wing ($E=10.6\times10^6$ psi) with

$$\frac{c}{t}=312.5,\quad \frac{t}{c}\left(\frac{E\beta}{q}\right)^{1/3}=\left(\frac{3}{\lambda_{cr}}\right)^{1/3};\quad \left(\frac{t}{h_0}\right)^2=0.$$

replotted as a function of the square of the frequency ratio $\omega_T/\omega_{1,S}$ in figure 5. The frequency ω_T is the rigid-body torsional or pitching frequency of the idealized structure, whereas $\omega_{1,S}$ is the frequency of the first symmetrical camber mode. The uncoupling of the rigid-body transverse mode $\omega_{0,S}$ motivated the choice of ω_T for use in the nondimensional frequency ratio. Thus,

$$\left(\frac{\omega_T}{\omega_{1,S}}\right)^2=\frac{\frac{K_T}{I_p\rho}}{\frac{16EI\alpha_{1,S}^4}{c\rho t}}=\frac{9}{4}\frac{k}{E\alpha_{1,S}^4}\left(\frac{c}{t}\right)^3 \tag{39}$$

where

$$K_T=2k\left(\frac{c}{2}\right)^2 \tag{40}$$

$$I=\frac{t^3}{12} \tag{41}$$

and the approximate polar moment of inertia I_p is given by

$$I_p\approx I_{ww}=\frac{2tc^3}{12} \tag{42}$$

Note from the curves presented in figure 5 that the torsional beam stiffness of the prototype as represented by ω_T is relatively unimportant for large values of ω_T and furthermore that flutter will occur even when ω_T is infinite $\left(\text{three-term solution, } \frac{t}{c}\left(\frac{E\beta}{q}\right)^{1/3}=0.3485\right)$. The reversal of the curve at $\left(\frac{\omega_T}{\omega_{1,S}}\right)^2=2.1$ (or $k=145$) for the three-term Galerkin approximation is similar to that occurring in other solutions that use three-mode approximations such as flat-panel modal solutions as shown in reference 7. For values of $\left(\frac{\omega_T}{\omega_{1,S}}\right)^2>2.1$ the

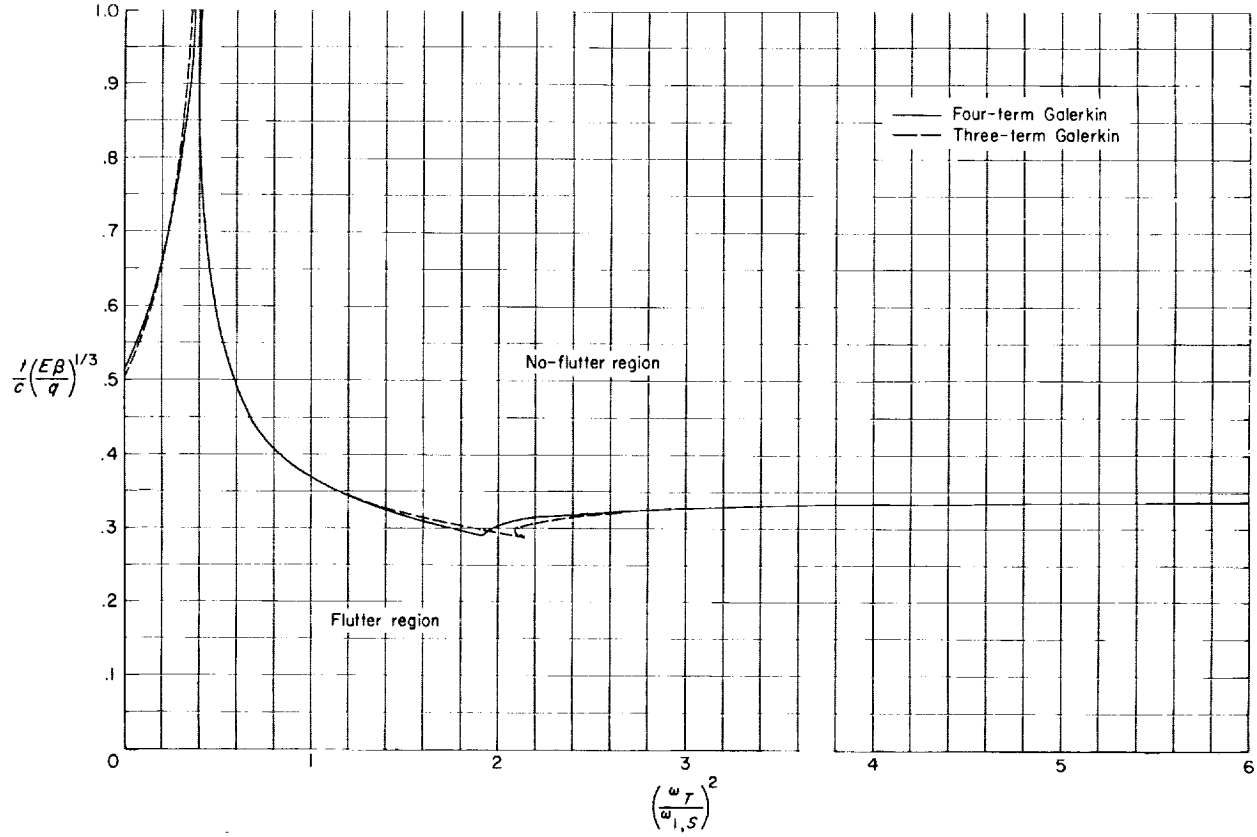

Figure 5.—Variation of the flutter parameter, $\frac{l}{c}\left(\frac{E\beta}{q}\right)^{1/3}$ with $\left(\frac{\omega_T}{\omega_{1,S}}\right)^2$ for $E=10.6\times10^6$ psi and $\frac{c}{l}=312.5$. $\left(\frac{l}{h_0}\right)^2=0$.

critical flutter boundary is defined by the coalescence of the rigid-body torsional (first antisymmetrical) and the first symmetrical chordwise mode while for $\left(\frac{\omega_T}{\omega_{1,S}}\right)^2<2.1$ the first symmetric and second antisymmetrical chordwise modes coalesce. (See fig. 6(a).) As $\left(\frac{\omega_T}{\omega_{1,S}}\right)^2$ is further decreased, a point is reached at which the second antisymmetric chordwise frequency becomes equal to the first symmetric chordwise frequency for zero airflow; at this point it appears as though flutter will occur at zero dynamic pressure. This phenomenon is quite common in flutter investigations and is probably due to the neglect of aerodynamic damping.

Four-term solution.—In order to investigate the accuracy in the region of the curve reversal and also the convergence of the three-term approximation, a four-term Galerkin solution was performed. For a four-term approximation in which the first two antisymmetrical chordwise modes (one of which is predominantly rigid-body torsion) and the first two symmetrical chordwise modes (the rigid-body transverse mode having become uncoupled in the solution) are considered, the determinant of equations (36) upon expansion reduces to a quadratic in Λ^2. Solving for the critical value of Λ by varying α results in two peaks, the minimum peak being Λ_{cr}.

The correlation between these approximate solutions and the exact solution for the specific case of pin-ended constraint conditions and $\left(\frac{t}{h_0}\right)^2=0$ is shown in figure 2. The agreement between the three- and four-term approximations and the exact solution is excellent, the critical flutter parameter being calculated as 70.5 for the three-term solution, 70.72 for the four-term solution, and 70.9 for the exact solution. In fact, the values of the curves as calculated for the first coalescing modes are so close that the curves

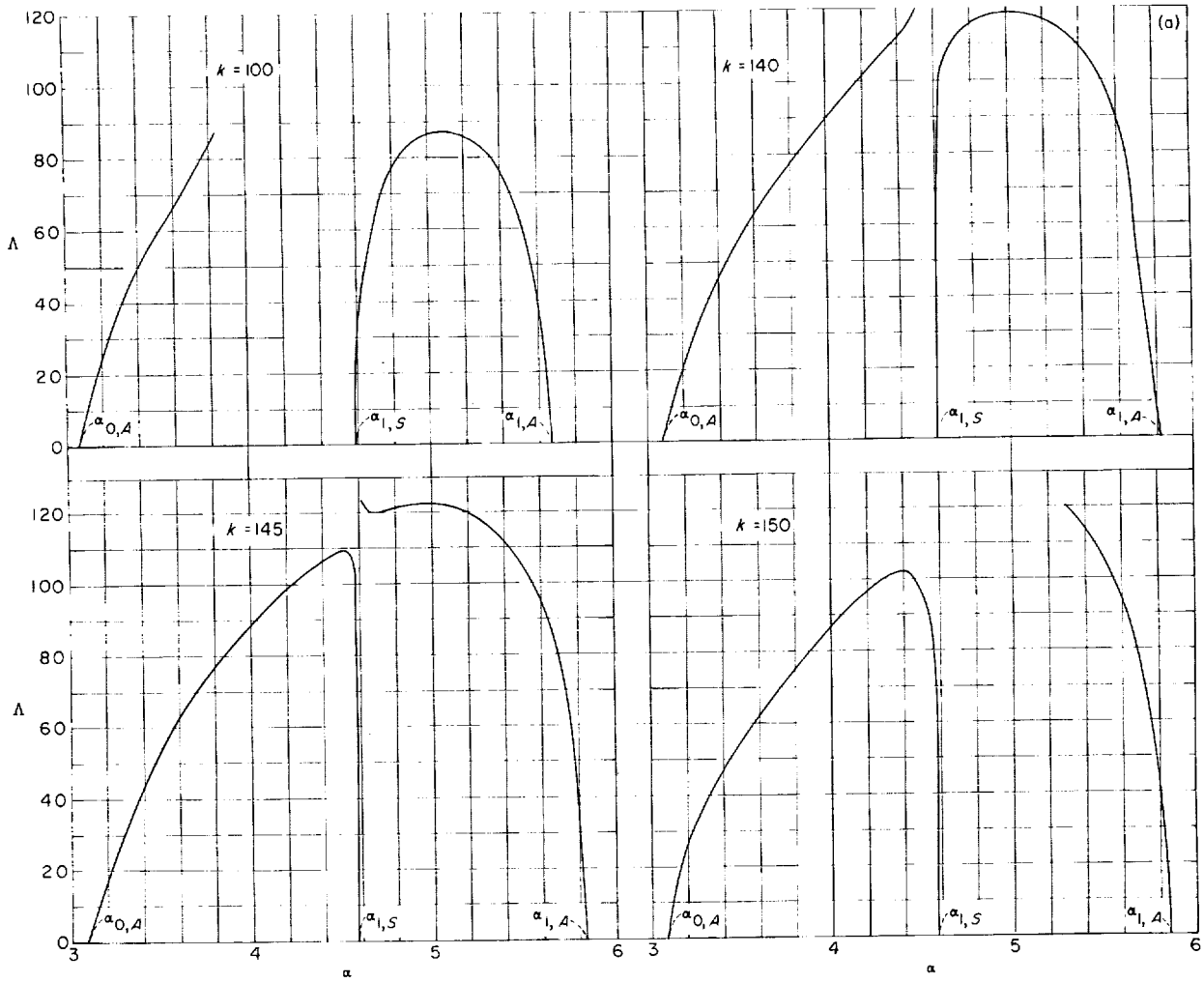

(a) Three-term Galerkin solution.

Figure 6.—Dynamic-pressure parameter Λ as a function of α for various values of k with $\left(\frac{t}{h_0}\right)^2=0$. $\frac{c}{t}=312.5$; $E=10.6\times10^6$ psi.

drawn through them cannot be easily distinguished one from another. The difference between the exact peaks and the approximate peaks becomes evident only at the higher coalescing modes. This agreement demonstrates the degree of excellence in comparison between the approximate Galerkin procedures and the exact solution for the special case of infinite k.

For the case of finite k the rapid convergence of the Galerkin procedures using only three and four modes, as is shown in figures 4 and 5, indicated that the inclusion of more terms in the approximate solution was not necessary in order to obtain accurate results.

Now that the accuracy of the Galerkin procedure has been evaluated it is of interest to examine more closely the behavior of the participating modes in the vicinity of the curve reversals shown in figures 4 and 5. In order to illustrate the change in coalescing modes, Λ has been plotted as a function of α for different values of k in figure 6(a) for the three-term approximation and in figure 6(b) for the four-term approximation. By following the sequence of plots in figure 6(a) for different values of k it can be seen that as the value of k varies the magnitude and shape of the

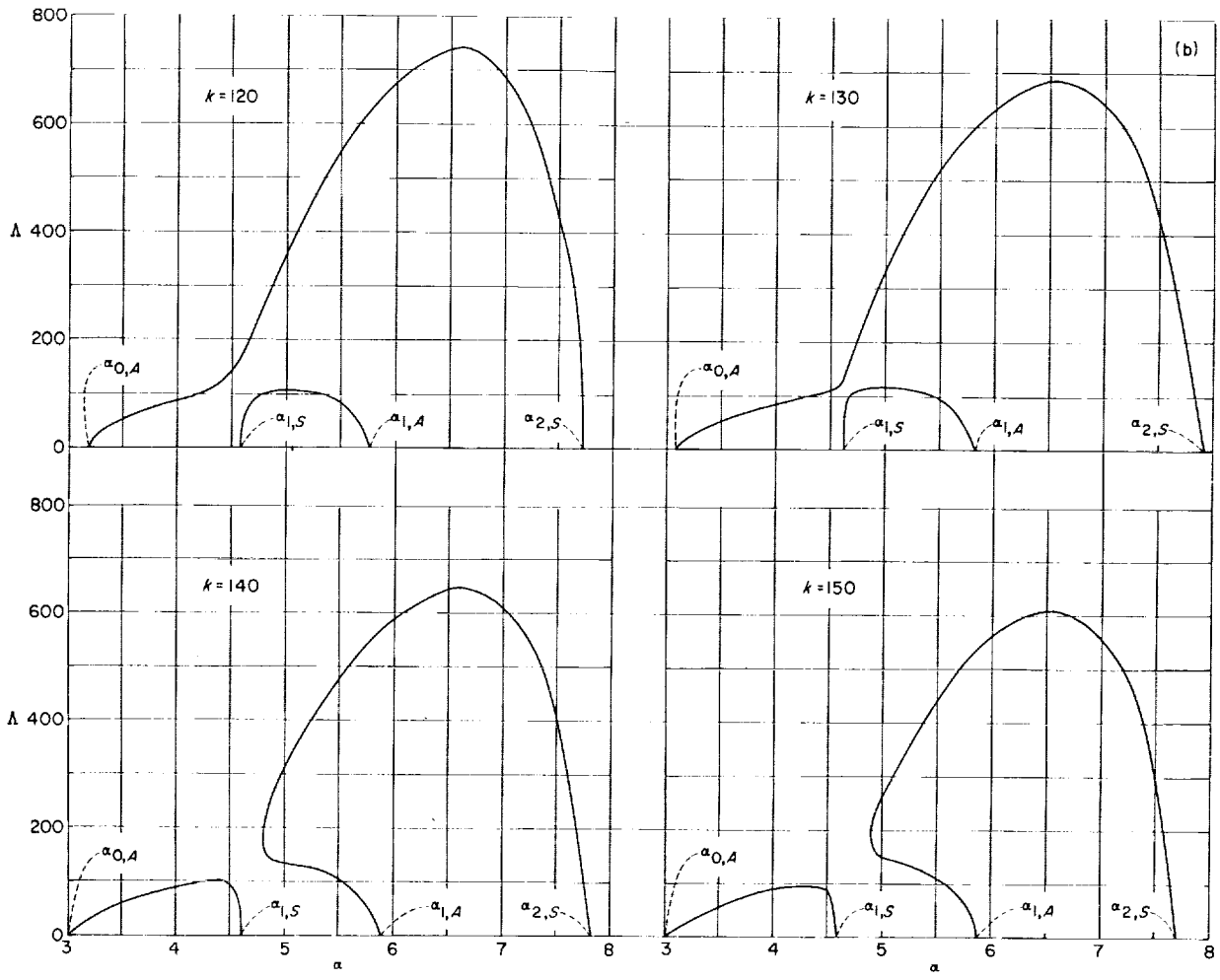

(b) Four-term Galerkin solution.

FIGURE 6.—Concluded.

peak changes until different modes coalesce. As was previously discussed the reversal of the curve for the three-term approximation was to be expected because of the cubic nature of the expanded determinant, as was demonstrated in flat-panel modal solutions. (See ref. 7.) The abrupt change in the curve for the four-term approximation shown in figure 5 occurring at $\left(\frac{\omega_T}{\omega_{1,S}}\right)^2=1.93$ ($k=133$) is somewhat surprising, however. This abrupt change for the four-term approximation is due to the type of modal coalescence illustrated in the sequence of plots in figure 6(b). In figure 6(b), as in figure 6(a), the variance in k causes a change in the magnitude and shape of the two peaks until different modes coalesce. The coalescence at values of $\left(\frac{\omega_T}{\omega_{1,S}}\right)^2>1.93$ occurs between the rigid-body torsional (first antisymmetrical) and the first symmetrical chordwise mode, and between second symmetrical and second antisymmetrical chordwise mode. When the value of k decreases until $\frac{\omega_T}{\omega_{1,S}}<1.93$, then the rigid-body torsional mode coalesces with the second symmetrical chordwise mode and beneath this curve the second antisymmetrical and first symmetrical chordwise modes coalesce, the smaller of these two peaks yielding Λ_{cr} as always.

Effects of variation in chord-thickness ratio.—In the previous Galerkin procedures the ratio of the chord to the skin thickness c/t was held

constant at 312.5, the value computed from the physical characteristics of the multiweb wings investigated in references 1 and 3.

In order to show the effect of variance in the ratio c/t on the flutter criterion, values of $\frac{t}{c}\left(\frac{E\beta}{q}\right)^{1/3}$ computed from the four-term approximation were plotted as a function of $\left(\frac{\omega_T}{\omega_{1,S}}\right)^2$ in figure 7 for three values of c/t. The values of c/t were taken as 500, 312.5, and 246.9, values consistent with practical design considerations and within the limits of the present idealization for monocoque and multiweb wings. As can be seen from figure 7, very little effect is noted in the flutter boundary caused by variations in c/t.

Effects of aerodynamic damping.—In both the exact analysis and in the Galerkin approximations aerodynamic damping has been neglected. The damping term was neglected in the exact analysis in order that a simplified solution to the differential equation could be found. For the Galerkin approximations, however, the inclusion of the aerodynamic damping term does not create any difficulties. Thus, the effect of aerodynamic damping on the critical flutter parameter has been investigated for the limiting conditions of pin-ended ($k=\infty$) and free-free ($k=0$) constraints by using a Galerkin modal approach.

A two-term Galerkin approximation (which is identical to the three-term approximation at $k=0$) was employed for the sake of simplicity, since the choice of the proper coupling modes has already been established. It is assumed therefore that the critical coupling modes do not change with the inclusion of aerodynamic damping and that only the magnitude of the critical Λ is affected.

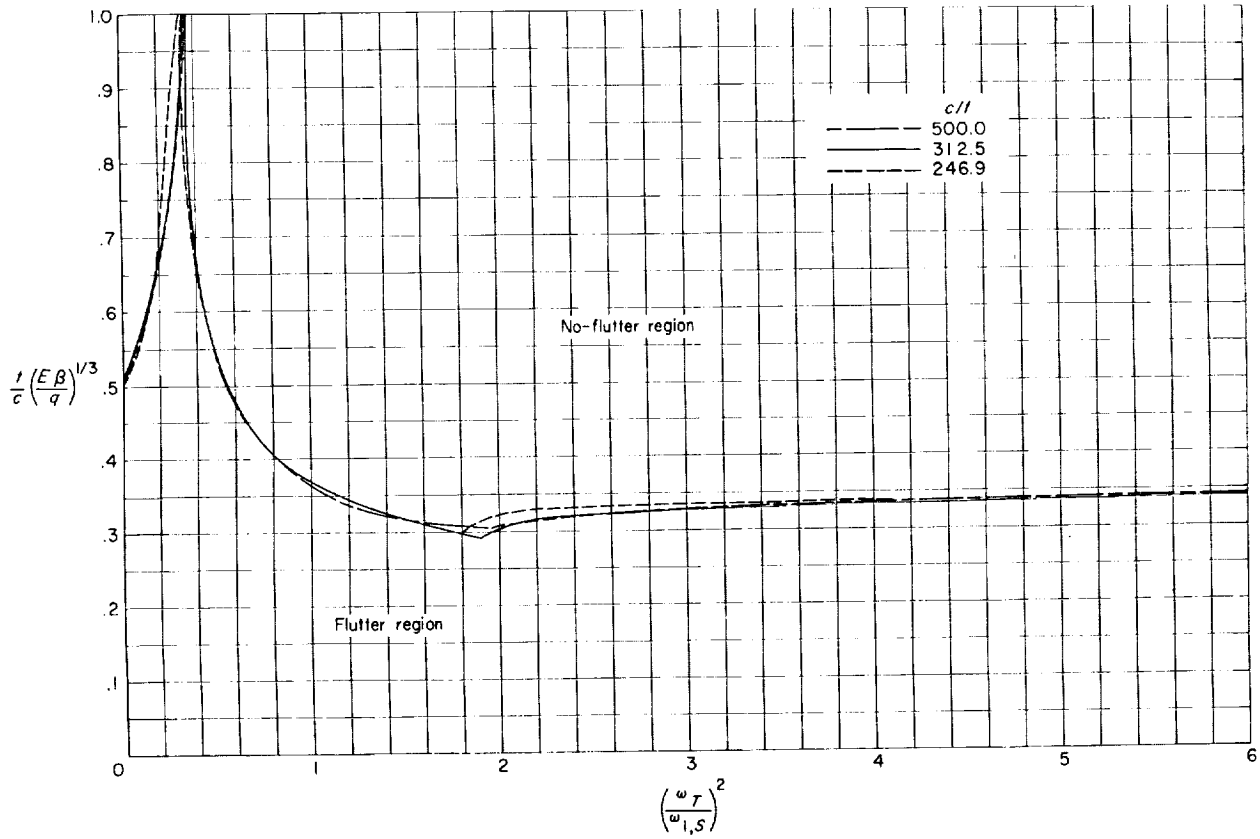

Figure 7.—Variation of flutter parameter $\frac{t}{c}\left(\frac{E\beta}{q}\right)^{1/3}$ with $\left(\frac{\omega_T}{\omega_{1,S}}\right)^2$ for various values of $\frac{c}{t}$ with $\left(\frac{t}{h_0}\right)^2=0$ and $E=10.6\times10^6$ psi.

The determinant of the coefficients (which are now complex) for the two-term Galerkin approximation reduces to

$$\begin{vmatrix} (\alpha_{n,S}^4+B^4)\int_{-1}^{1} w_{n,S}^2\,d\xi & -\Lambda\int_{-1}^{1} w_{m,A}w'_{n,S}\,d\xi \\ \Lambda\int_{-1}^{1} w_{m,A}w'_{n,S}\,d\xi & (\alpha_{m,A}^4+B^4)\int_{-1}^{1} w_{m,A}^2\,d\xi \end{vmatrix}=0 \tag{43}$$

where B^4 is now complex and is given by equation (13) and $w_{n,S}$ and $w_{m,A}$ are the general vibration modes for $\left(\frac{t}{h_0}\right)^2\neq 0$.

For $k=\infty$, the first antisymmetrical (rigid-body torsional, $m=0$) and the first symmetrical chordwise ($n=1$) modes should be used in equation (43).

For $k=0$ the first antisymmetrical mode is zero and uncouples from the solution; the second antisymmetrical ($m=1$) and the first symmetrical chordwise ($n=1$) modes should be used in this case.

If B^4 is complex and ω is considered real, expanding and simplifying equation (43) and equating the coefficients of both the real and imaginary parts to zero yields the following expression for Λ_{cr}:

$$\Lambda_{cr}=\frac{1}{128K_1}\left[\eta(\alpha_{n,S}^4+\alpha_{m,A}^4)+\sqrt{\eta^2(\alpha_{n,S}^4+\alpha_{m,A}^4)^2+128K_1(\alpha_{n,S}^4-\alpha_{m,A}^4)^2}\right] \tag{44}$$

where

$$\eta=\frac{1}{2}\left(\frac{c}{t}\right)_\rho\sqrt{M^2-1}\,\frac{\rho_\infty}{\rho} \tag{45}$$

and

$$K_1=\frac{\alpha_{n,S}^4}{\alpha_{n,S}^4-\alpha_{m,A}^4}\left\{\alpha_{m,A}\coth\alpha_{m,A}\left[\frac{1}{\frac{\alpha_{n,S}^4}{48}\left(\frac{t}{h_0}\right)^2+1}\right]-1\right\}\left(\left[1-\frac{1}{\frac{\alpha_{n,S}^4}{48}\left(\frac{t}{h_0}\right)^2+1}\right]+\frac{\alpha_{n,S}^4}{\alpha_{m,A}^4-\alpha_{n,S}^4}\left\{1-\alpha_{m,A}\coth\alpha_{m,A}\left[\frac{1}{\frac{\alpha_{n,S}^4}{48}\left(\frac{t}{h_0}\right)^2+1}\right]\right\}\right)\div\left\{\tan^2\alpha_{n,S}-\tanh^2\alpha_{n,S}+2+\frac{2}{\frac{\alpha_{n,S}^4}{48}\left(\frac{t}{h_0}\right)^2+1}\left[3-\frac{4}{\frac{\alpha_{n,S}^4}{48}\left(\frac{t}{h_0}\right)^2+1}\right]\right\} \tag{46}$$

In order to arrive at numerical results of the effects of aerodynamic damping on the flutter parameter Λ in the present investigation, the data from the flutter failures of the multiweb-wing structures were used. The pertinent parameters used in some of these tests are tabulated below:

$$\frac{c}{t}=312.5$$

$$\left(\frac{t}{h_0}\right)^2=0.0187$$

$$\frac{\rho_\infty}{\rho}=0.0001453$$

$$E=10.6\times10^6\text{ psi}$$

$$M=3.0$$

The results obtained by using the tabulated data indicate that for $k=0$ and $\left(\frac{t}{h_0}\right)^2=0$ ($\alpha_{1,S}=4.591$; $\alpha_{1,A}=3.927$), the effect of aerodynamic damping increases Λ_{cr} by only 0.3 percent. If the actual $\left(\frac{t}{h_0}\right)^2$ value of 0.0187 is used in place of the approximation, $\left(\frac{t}{h_0}\right)^2=0$, the results are not altered; the increase in Λ_{cr} is still only of the order of 0.3 percent.

When $k=\infty$ and $\left(\frac{t}{h_0}\right)^2=0$ ($\alpha_{1,S}=4.591$; $\alpha_{0,A}=\pi$), the effect of aerodynamic damping on Λ_{cr} is still negligible, the value of Λ_{cr} being increased by only 0.2 percent. A greater effect would be realized in these limiting cases, however, if the c/t ratios increased, as can be seen from the density-ratio

factor η in equation (45). Note that the effects of damping have been studied only for the limiting cases of $k=0$ and $k=\infty$. It is nevertheless believed that the conclusions based on these cases are applicable for finite values of k except in the questionable region of $\left(\frac{\omega_T}{\omega_{1,S}}\right)^2 \approx 0.35$, where flutter appears to occur for negligible air flow.

APPLICATION OF METHOD

The previous sections discussed the flutter behavior of an idealized structure. The purpose of the present section is to show how these results can be used to predict the flutter boundary of the multiweb wings used in the experimental investigations. In addition, the accuracy of the predicted flutter boundary is ascertained by comparison with actual flutter data.

TEST SPECIMENS

In the experimental investigation into the dynamic flutter failures of multiweb-wing structures, a series of multiweb wings were tested in the preflight jet at the NASA Wallops Station at a Mach number of 2 (see refs. 1 to 3) and in the Langley 9- by 6-foot thermal structures tunnel at a Mach number of 3. Specimen identification (see table II) conforms with that of the multiweb-wing (MW) series previously discussed in references 1 to 3. Numbers within parentheses indicate duplicates of the same specimen. For example, MW–2–(2) identifies the second MW–2 model tested. These aluminum-alloy ($E=10.6\times10^6$ psi) multiweb models had 5-percent-thick circular-arc airfoil sections with solid leading and trailing edges as shown in figure 1(a). The chord length of 15 of the 18 models tested (models MW–2 and MW–4) was 20 inches and the skin thickness t, 0.064 inch; thus the ratio c/t for these specimens was 312.5. These models had a 20-inch span (approximately) with solid root and tip bulkheads but were free of internal ribs. (The models designated MW–2 had 0.25-inch tip bulkheads and those designated MW–4 had 0.025-inch tip bulkheads.) The parameter $\left(\frac{t}{h_0}\right)^2$ was 0.0187 and the wing aspect ratio slightly over 1.0.

The last three multiweb models listed in table II (designated MW–1–(2), MW–23, and MW–24) are presented in order to compare the theoretical flutter boundary with multiweb models of different chord length and skin thickness from those of models MW–2 and MW–4. The ratio c/t of these multiweb models, however, is quite similar to that of models MW–2 and MW–4 ($c/t=320$ to $c/t=312.5$ for MW–2–(4)). Model MW–1–(2) (from ref. 2)

TABLE II.—AERODYNAMIC TEST CONDITIONS

[$\rho=0.000259$ slug/cu in.]

Model	Mach number	Stagnation temperature, °F	Velocity, U_∞, fps	Air density, ρ_∞, slugs/cu ft	Dynamic pressure, q, lb/sq in.	Flutter	References
MW–2–(2)	1.99	89	1,700	0.003610	36.40	Yes	1
MW–2–(2)	1.99	540	2,300	.002290	42.00	Yes	1
MW–2–(2)	1.99	503	2,260	.002320	41.10	Yes	1
MW–2–(2)	1.99	517	2,280	.002300	41.50	Yes	1
MW–2–(2)	1.99	474	2,230	.002380	40.90	Yes	1
MW–2–(2)	1.99	525	2,290	.002300	41.80	Yes	1
MW–2–(4)	1.99	551	2,314	.002220	41.44	Yes	3
MW–4–(3)	1.99	531	2,288	.002280	41.58	Yes	3
MW–4–(4)	3.00	651	2,928	.001095	32.62	Yes	Unpublished data
MW–4–(5)	3.00	301	2,423	.001640	33.49	No	Unpublished data
MW–4–(5)	3.00	395	2,369	.001423	32.62	No	Unpublished data
MW–4–(6)	3.00	502	2,727	.001315	33.89	No	Unpublished data
MW–4–(6)	3.00	608	2,871	.001183	33.89	No	Unpublished data
MW–4–(7)	3.00	673	2,961	.001140	34.71	Yes	Unpublished data
MW–4–(9)	3.00	659	2,943	.000786	23.62	No	Unpublished data
MW–1–(2)	1.99	574	2,350	.002120	40.60	Yes	2
MW–23	3.00	647	2,923	.001140	33.82	No	Unpublished data
MW–24	3.00	656	2,935	.001077	32.24	Yes	Unpublished data

has a 40-inch chord, skin thickness of 0.125, tip bulkhead of 1 inch, and a span of 37.50 inches. Model MW–23 has the same dimensions as MW–1–(2) except for a tip bulkhead of 0.051 inch and a span of 43.25 inches. Model MW–24 has a 60-inch chord, skin thickness of 0.188, tip bulkhead of 0.073 inch, and a span of 64.88 inches. The ratio $\left(\frac{t}{h_0}\right)^2$ for the three models is 0.0178 ($\alpha_{1,S}=4.568$) and the wing aspect ratio is approximately 1.0.

Tabulated in table II are such pertinent parameters of the experimental tests of these models as Mach number, stagnation temperature, velocity and density of the jet stream, and dynamic pressure. Whether or not flutter occurred is indicated. The published references from which data were obtained are listed in case more information is desired.

EXPERIMENTAL RESULTS

Although all the multiweb wings had 5-percent-thick circular-arc cross sections, the curvature of these cross sections can be very accurately approximated by the parabolic equation $h=h_0(1-\xi^2)$. Furthermore, the ratio c/t of the MW–2 and MW–4 multiweb wings is 312.5 and thus the theoretical flutter boundary presented in figure 5 (for the four-term approximation) is the predicted flutter boundary for 15 of the experimental models and is again shown in figure 8. In figure 8 are also shown the experimental flutter points tabulated in table III for all the MW models. (Note from table III and fig. 8 that some of the flutter points fall in such close proximity to each other that they are not easily distinguished.) In order to tabulate the experimental flutter points the values of the first torsional frequency ω_T and the first symmetrical chordwise frequency $\omega_{1,S}$ must be known. The first torsional frequency ω_T was determined experimentally and is listed in the first column of table III. The constant value of $\omega_{1,S}$ was determined from equation (24) once $\alpha_{1,S}$ was found from the general symmetrical frequency equation (given in ref. 4 for any value of $\left(\frac{t}{h_0}\right)^2$) to be 4.566.

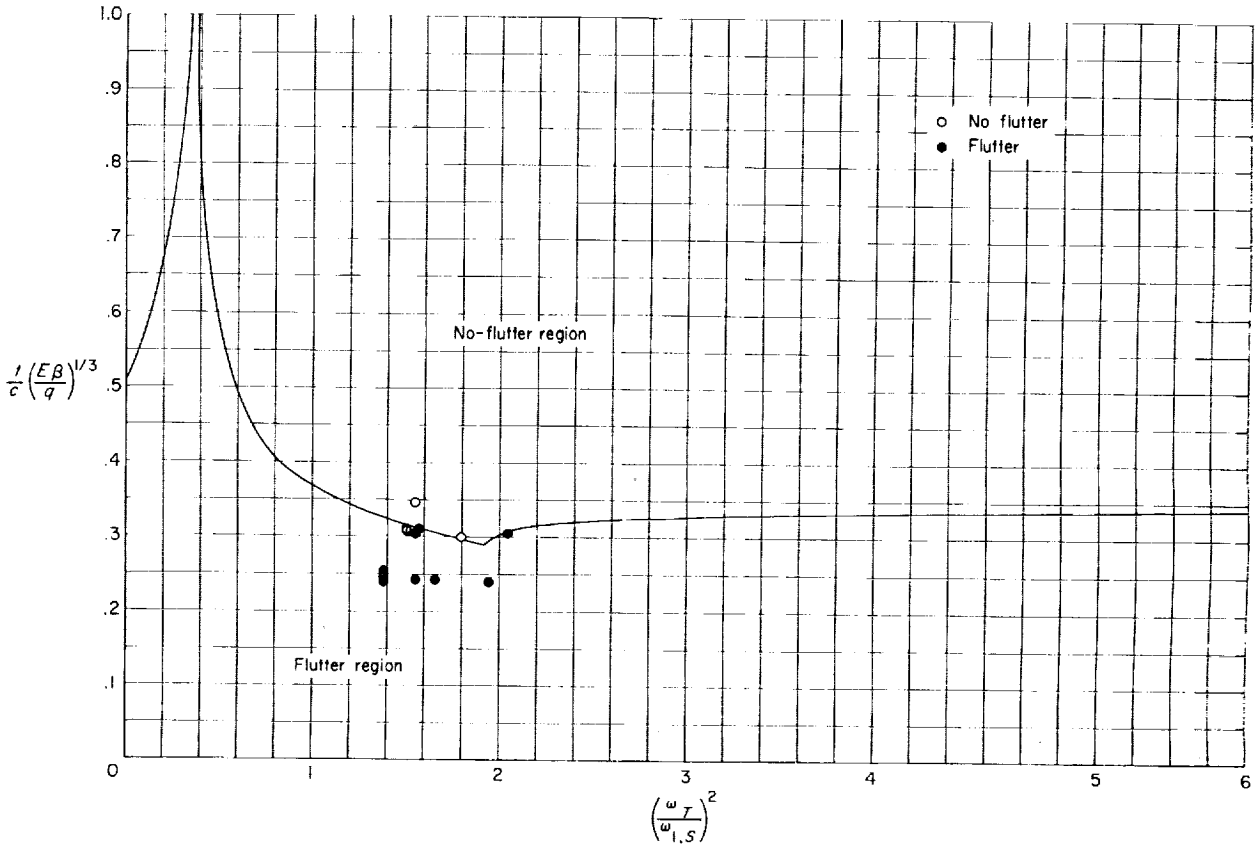

FIGURE 8. Comparison of theoretical flutter boundary with experimental data. $c/t=312.5$.

TABLE III.—VIBRATION CHARACTERISTICS FOR FLUTTER SPECIMENS

[ρ=0.000259 slug/cu in.]

Model	ω_T, exp.	I_p, in.^{5}	k, lb/in.	$\left(\frac{\omega_T}{\omega_{1,S}}\right)^2$	$\frac{t}{c}\left(\frac{E\beta}{q}\right)^{1/3}$
MW-2-(2)	139	98. 135	92. 76	1. 3824	0. 2542
MW-2-(2)	139	98. 135	92. 76	1. 3824	. 2423
MW-2-(2)	139	98. 135	92. 76	1. 3824	. 2441
MW-2-(2)	139	98. 135	92. 76	1. 3824	. 2433
MW-2-(2)	139	98. 135	92. 76	1. 3824	. 2445
MW-2-(2)	139	98. 135	92. 76	1. 3824	. 2427
MW-2-(4)	147	98. 135	103. 77	1. 5465	. 2434
MW-4-(3)	149	98. 135	111. 39	1. 6600	. 2431
MW-4-(4)	145	98. 135	105. 49	1. 5721	. 3111
MW-4-(5)	142	98. 135	101. 17	1. 5077	. 3084
MW-4-(5)	142	98. 135	101. 17	1. 5077	. 3111
MW-4-(6)	143	98. 135	102. 60	1. 5290	. 3072
MW-4-(6)	143	98. 135	102. 60	1. 5290	. 3072
MW-4-(7)	144	98. 135	104. 04	1. 5505	. 3047
MW-4-(9)	144	98. 135	104. 04	1. 5505	. 3465
MW-1-(2)	74	1737. 91	121. 62	1. 9428	. 2393
MW-23	76	1525. 53	112. 62	1 7990	. 3002
MW-24	54	7798. 21	129. 17	2. 0468	. 3058

The spring constants k were computed from the first torsional frequency by the well-known relation

$$\omega_T^2=\frac{K_T}{\rho I_p} \tag{47}$$

where K_T is the torsional spring constant and I_p is the polar moment of inertia per unit length in the spanwise direction. From equation (40)

$$K_T=2k\left(\frac{c}{2}\right)^2$$

Thus

$$k=\frac{2\omega_T^2\rho I_p}{c^2} \tag{48}$$

As can be seen from figure 8 the predicted flutter boundary and the experimental flutter points agree quite well. Some of the experimental no-flutter points do fall slightly below the flutter boundary in the flutter region, but it is believed that this may be due to the omission of temperature considerations in the calculated flutter boundary. The heated air of the test facilities produces a temperature gradient between the skin and webs of the multiweb model inducing thermal stresses. No attempt has been made to include these thermal stresses in the present analysis. (The inclusion of thermal effects would necessitate applying another set of elastic restraints horizontally, at the leading and trailing edges of the wing cross section, fig. 1(b), since the edges are assumed to remain stationary in the present analysis.) However, the magnitude of the effect of these thermal stresses on the flutter behavior of the multiweb wings is not too evident from a comparison of the experimental data and the theoretically predicted flutter boundary.

CONCLUDING REMARKS

The flutter characteristics determined from an idealized model have been used successfully to predict camber or cross-sectional flutter behavior of actual multiweb and monocoque wings of low aspect ratio. The use of modified piston theory for the air loads in the flutter analysis yielded flutter results that agreed well with existing experimental data. An approximate three- and four-term Galerkin procedure utilizing the exact modes and frequencies of the vibrational analysis of these multiweb wings was employed to establish the flutter boundary. The correlation between this approximate solution and an exact solution for the specific case of simply supported end constraints indicated that the inclusion of more terms in the approximate modal solution was not necessary, the three- and four-term approximations being

within a few percent of the exact. This agreement was also borne out by the rapid convergence of the Galerkin procedures for the three- and four-term approximations.

The existence of curvature in a wing cross section was shown to have an appreciable effect on the flutter criterion. Once the curvature is present, however, variations in the degree of curvature were shown to have little effect on the flutter boundary. The effects of aerodynamic damping on the flutter boundary were investigated for the limiting cases of $k=0$ and $k=\infty$ and found to be negligible.

The influence of thermal stresses arising in the multiweb-wing structure due to heating of the skins by the hot-air jet have not been considered in the present analysis, but a comparison of the experimental data with the theoretically predicted flutter boundary did not indicate the results to be unduly affected by thermal stresses.

LANGLEY RESEARCH CENTER,
NATIONAL AERONAUTICS AND SPACE ADMINISTRATION,
LANGLEY STATION, HAMPTON, VA., *August 23, 1962.*

APPENDIX

EXACT SOLUTION OF DIFFERENTIAL EQUATION FOR $k=\infty$ AND AERODYNAMIC DAMPING NEGLECTED

An exact solution to equation (8), as given in the text, can be obtained directly by neglecting aerodynamic damping. In a manner similar to that employed by Hedgepeth in reference 6, an exact solution is obtained for the limiting case of pin-ended constraints ($k=\infty$) at the leading and trailing edges of the cross section. With aerodynamic damping neglected, B^4 reduces to $-\alpha^4$ and equation (8) can be written as

$$w^{IV}+\Lambda w'-\alpha^4 w=\frac{-6\lambda h_0 c^2}{Et^3} \tag{A1}$$

Furthermore, the origin of the coordinate axes is moved to the leading edge of the cross section both to aid in a later comparison with the infinite-aspect-ratio simply supported plate and to simplify somewhat the form of the solution to equation (A1). Thus

$$\psi=\xi+1 \tag{A2}$$

and the expression for the half-depth h can be written as

$$h=h_0\left[1-(\psi-1)^2\right] \tag{A3}$$

The associated boundary conditions for the pin-ended constraints become

$$w(0)=w(2)=0 \tag{A4}$$

$$\left.\frac{d^2w}{d\psi^2}\right|_{\psi=0}=\left.\frac{d^2w}{d\psi^2}\right|_{\psi=2}=0 \tag{A5}$$

The normal midplane force λ is considered constant and equal to the average midplane force as given by equation (15) or, since $w(0)=w(2)=0$, simply reduces to

$$\lambda=\frac{4h_0Et}{c^2}\int_0^2 w\,d\psi \tag{A6}$$

The solution to equation (A1) can be written in the form

$$w=\frac{6\lambda h_0 c^2}{\alpha^4 Et^3}+\sum_{p=1}^{4} A_p e^{m_p\psi} \tag{A7}$$

where m_p (for $p=1$ to 4) are the roots of the auxiliary equation

$$m^4+\Lambda m-\alpha^4=0 \tag{A8}$$

Since ω is considered real, α^4 is always positive and Λ is always positive by definition; hence, m has one possible real positive root and one possible real negative root and a pair of complex roots, or two pairs of complex roots.

Let

$$\left.\begin{aligned} m_1&=\theta+\phi\\ m_2&=\theta-\phi\\ m_3&=\gamma+i\delta\\ m_4&=\gamma-i\delta \end{aligned}\right\} \tag{A9}$$

In order for these roots (eqs. (A9)) to satisfy equation (A8), the following equations must be true

$$m_1+m_2+m_3+m_4=0 \tag{A10}$$

$$m_1m_2+m_3m_4+(m_1+m_2)(m_3+m_4)=0 \tag{A11}$$

$$m_1m_2(m_3+m_4)+m_4m_3(m_1+m_2)=-\Lambda \tag{A12}$$

$$m_1m_2m_3m_4=-\alpha^4 \tag{A13}$$

By substitution of the relations for m_1, m_2, m_3, and m_4 given in equations (A9) into equations (A10) to (A13) the following relationships between γ, δ, ϕ, and θ are found:

$$\gamma=-\theta \tag{A14}$$

$$\delta^2=\phi^2+2\theta^2 \tag{A15}$$

$$2\theta(\phi^2+\delta^2)=-\Lambda \tag{A16}$$

$$(\theta^2-\phi^2)(\theta^2+\delta^2)=-\alpha^4 \tag{A17}$$

By inspection of equations (A14) to (A17) it can be seen that

$$\left.\begin{aligned} &\theta<0\\ &|\phi|>|\theta| \end{aligned}\right\} \tag{A18}$$

while from equation (A17) the possibility of two pairs of complex roots is eliminated. Substitution of equation (A15) into equations (A16) and

(A17) yields, after some algebraic manipulation,

$$\phi^2=-\theta^2-\frac{\Lambda}{4\theta} \tag{A19}$$

and

$$\theta^6+\frac{1}{4}\alpha^4\theta^2-\frac{\Lambda^2}{64}=0 \tag{A20}$$

In equation (A20), θ^2 has one positive real root and two conjugate complex roots. However, interest is centered in the case where θ is real and negative (eq. (A18)); hence θ^2 is real and positive. Substitution for ϕ^2 from equation (A19) into equation (A15) yields

$$\delta^2=\theta^2-\frac{\Lambda}{4\theta} \tag{A21}$$

Therefore, for the flutter analysis, equation (A7) can be written as

$$w=\frac{6\lambda h_0 c^2}{\alpha^4 E t^3}+e^{\theta\psi}(C_1\cosh\phi\psi+C_2\sinh\phi\psi)+e^{-\theta\psi}(C_3\cos\delta\psi+C_4\sin\delta\psi) \tag{A22}$$

Substitution of the general solution (given by eq. (A22)) into the pin-ended boundary conditions (eqs. (A4) and (A5)) yields the following set of equations for the coefficients C_1, C_2, C_3, and C_4:

$$\frac{6\lambda h_0 c^2}{\alpha^4 E t^3}+C_1+C_3=0 \tag{A23}$$

$$\frac{6\lambda h_0 c^2}{\alpha^4 E t^3}+C_1 e^{2\theta}\cosh 2\phi+C_2 e^{2\theta}\sinh 2\phi+C_3 e^{-2\theta}\cos 2\delta+C_4 e^{-2\theta}\sin 2\delta=0 \tag{A24}$$

$$C_1(\theta^2+\phi^2)+C_2 2\theta\phi+C_3(\theta^2-\delta^2)-C_4 2\theta\delta=0 \tag{A25}$$

$$C_1[(\theta^2+\phi^2)e^{2\theta}\cosh 2\phi+2\theta\phi e^{2\theta}\sinh 2\phi]+C_2[2\theta\phi e^{2\theta}\cosh 2\phi+(\theta^2+\phi^2)e^{2\theta}\sinh 2\phi]+C_3[(\theta^2-\delta^2)e^{-2\theta}\cos 2\delta+2\theta\delta e^{-2\theta}\sin 2\delta]-C_4[2\theta\delta e^{-2\theta}\cos 2\delta-(\theta^2-\delta^2)e^{-2\theta}\sin 2\delta]=0 \tag{A26}$$

where λ is written as

$$\lambda=-\frac{1}{2\theta\left(\frac{c^2}{8Eth_0}-\frac{6h_0c^2}{Et^3\alpha^4}\right)}\left\{C_1\left[\frac{e^{2\theta}\left(\cosh 2\phi-\frac{\phi}{\theta}\sinh 2\phi\right)-1}{1-\left(\frac{\phi}{\theta}\right)^2}\right]+C_2\left[\frac{e^{2\theta}\left(\sinh 2\phi-\frac{\phi}{\theta}\cosh 2\phi\right)+\frac{\phi}{\theta}}{1-\left(\frac{\phi}{\theta}\right)^2}\right]+C_3\left[\frac{e^{-2\theta}\left(-\cos 2\delta+\frac{\delta}{\theta}\sin 2\delta\right)+1}{1+\left(\frac{\delta}{\theta}\right)^2}\right]+C_4\left[\frac{e^{-2\theta}\left(-\sin 2\delta-\frac{\delta}{\theta}\cos 2\delta\right)+\frac{\delta}{\theta}}{1+\left(\frac{\delta}{\theta}\right)^2}\right]\right\} \tag{A27}$$

For a nontrivial solution the determinant of the coefficients must equal zero. Substitution of λ given by equation (A27) into equations (A23) and (A24) and subsequent simplification yields the determinant of the coefficients in terms of θ, ϕ, δ, $\left(\frac{t}{h_0}\right)^2$, α^4, and Λ as shown in table I.

Note that if the half-depth h is equal to zero everywhere ($h_0=0$), the parabolic airfoil reduces to a flat beam and a in table I becomes zero. This modified determinant, when expanded, will yield an expression which is identical to that for the infinite-aspect-ratio simply supported plate solved exactly in reference 6.

REFERENCES

1. Miltonberger, Georgene H., Griffith, George E., and Davidson, John R.: Tests of Aerodynamically Heated Multiweb Wing Structures in a Free Jet at Mach Number 2—Two Aluminum-Alloy Models of 20-Inch Chord With 0.064-Inch-Thick Skin at Angles of Attack of 0° and ±2°. NACA RM L57H19, 1957.
2. Griffith, George E., and Miltonberger, Georgene H.: Tests of Aerodynamically Heated Multiweb Wing Structures in a Free Jet at Mach Number 2—An Aluminum-Alloy Model of 40-Inch Chord With 0.125-Inch-Thick Skin. NACA RM L58C24, 1958.
3. Trussell, Donald H., and Thomson, Robert G.: Tests of Aerodynamically Heated Multiweb Wing Structures in a Free Jet at Mach Number 2. Five Aluminum-Alloy Models of 20-Inch Chord With 0.064-Inch-Thick Skin, 0.025-Inch-Thick Webs, and Various Chordwise Stiffening at 2° Angle of Attack. NASA TM X–186, 1960.
4. Thomson, Robert G., and Kruszewski, Edwin T.: Cross-Sectional Deformations of Monocoque Beams and Their Effects on the Natural Vibration Frequencies. NASA TN D 987, 1961.
5. Johns, D. J.: The Influence of Panel Deformations on Wing Flutter. Jour. Aero/Space Sci. (Readers' Forum), vol. 27, no. 2, Feb. 1960, pp. 137–138.
6. Hedgepeth, John M.: On the Flutter of Panels at High Mach Numbers. Jour. Aero. Sci. (Readers' Forum), vol. 23, no. 6, June 1956, pp. 609–610.
7. Hedgepeth, John M.: Flutter of Rectangular Simply Supported Panels at High Supersonic Speeds. Jour. Aero. Sci., vol. 24, no. 8, Aug. 1957, pp. 563–573, 586.

U.S. GOVERNMENT PRINTING OFFICE: 1963